MECHANICS OF THE DISPLACEMENT PROCESS OF DRILLING MUDS BY CEMENT SLURRIES USING AN ACCURATE RHEOLOGICAL MODEL

ROBERT M. BEIRUTE
The Western Company of North America
RAYMOND W. FLUMERFELT
University of Houston

ABSTRACT

This paper deals with the development of a mathematical model to describe the miscible displacement of drilling muds by cement slurries under laminar flow conditions. The model accounts for the effects of differing properties, geometry, and displacement rates. The model assumes that "mixing" in the displacement zone by molecular diffusion is minimal, and uses the Robertson-Stiff model to describe the rheological properties of both the drilling fluid and the cement slurry.

The application of the model to a range of displacement conditions (densities, viscosities, yield stresses, displacement rates, etc.) indicates the conditions under which optimal or near optimal displacements are possible, and hence, provides a basis for designing efficient cementing operations from simple material property characterizations. Of special interest is the effect of the yield stress. These parameters are founded to strongly affect the displacement efficiency, particularly the formation of cement channels. Such results are described quantitatively in the paper. The effects of the other rheological properties, the densities, and the displacement rates are also described. Field application cases are also included in this paper.

INTRODUCTION

Although many papers have been written on the subject of drilling mud displacement from wellbores during cementing operations (see references, 1-11, for example), there are still many unresolved fundamental and practical questions. In particular, both laminar and turbulent flow conditions can produce good displacements[1,8-11]; however, it is still not clear which represents the most effective displacement mechanism. Also, the displacement achieved under laminar conditions can vary greatly, involved and the flow conditions. In some cases, depending on the material properties of the fluids very stable, high efficiency displacements are achieved, while in others, unstable fingering of the displacing phase occurs, resulting in extremely low-efficiency displacements. Even in the stable displacement cases, it has been only recently that efforts have been reported relating the displacement efficiency to the cement and mud material properties (densities and rheological properties) and the displacement rates.[2] In the unstable cases, turbulent flow displacement would probably be dictated, but, as yet, there is no basis for estimating the displacement expected under different rates, nor the amount of the displacing phase which would be required. Further, the critical conditions separating stable and unstable displacement regimes have only been partially defined, and these relate only to Newtonian fluids, whereas drilling fluids and cements are highly non-Newtonian.

It is clear that our knowledge of the fundamentals of the displacement processes in cementing is still quite limited, and, as a result, it is doubtful that many cementing operations are as effective or efficient as they might be if this information were available. Under normal conditions, satisfactory cement jobs are possible with sub-optimal displacements; however, under more demanding operations, such as displacement in permafrost zones, high-efficiency displacements of the water base fluids are required. Clearly, in these latter situations, a more accurate description of the displacement process is necessary, and such descriptions must influence the selection of the mud and cement properties to be used.

In the present paper, we cannot consider all of the questions just raised. Instead, we focus on those aspects relating to the dependence of laminar flow displacement efficiency on the densities and rheological properties and the displacement rates. The fluids are considered to be non-Newtonian, and the displacement zone is taken as the narrow gap annuli between concentric cylinders, or equivalently, the region between two parallel plates. The approach is analytical and similar to that used previously by Flumerfelt[2]; however, the rheological descriptions are more complete. Although the solution is approximate, it still provides a basis for analyzing mud displacement and for establishing those conditions most favorable for effective and efficient displacements during cementing.

THE PHYSICAL MODEL AND ASSUMPTIONS

The displacement process is assumed to take place as depicted in Figure 1. A well defined, stable penetrating front of the displacing fluid (cement slurry) is assumed to move through the displaced phase (mud) under laminar flow conditions. Since the desire here is the calculation of displacement efficiency (volume displaced at time t/volume of the flow field), the position of the penetrating front must be known at any time during the displacement process.

The exact analysis of such a problem would require the solution of the equations of motion and continuity for the velocity and pressure fields in

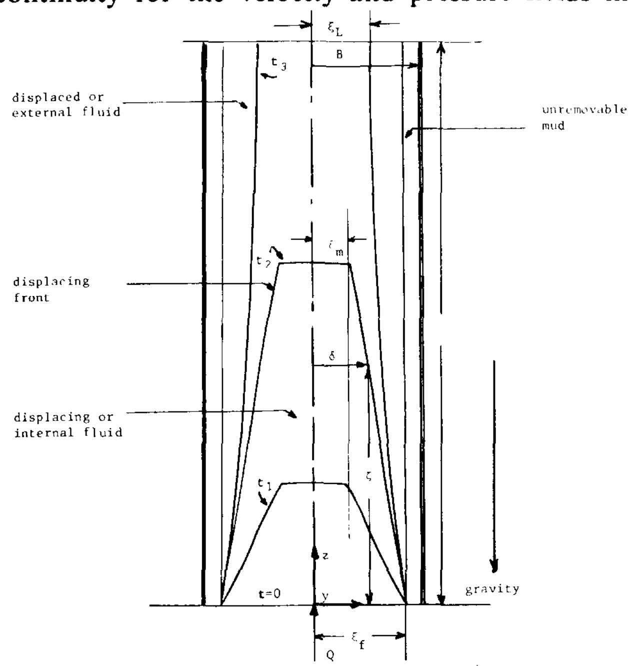

FIGURE 1—THE DISPLACEMENT PROCESS

each of the phases, i.e., $\underline{v} = (v_z(y,z,t), v_y(y,z,t)\ 0)$ and $p = p(y,z,t)$ for the displaced (or annular) phase, and $\underline{v} = (v_z\ (y,z,t),\ v_y\ (y,z,t),\ 0)$ and $\hat{p} = \hat{p}(y,z,t)$ for the displacing phase (the core fluid). The equations which result are non-linear, simultaneous, partial differential equations, for which exact analytical solution is not possible. Even numerical solutions of such problems for Newtonian fluids are quite involved.[12]

Here we utilize an approximate analysis similar to that used in lubrication problems[13] by focusing on maximum gradient effects. In particular, the following assumptions are employed.

1. The displacing and displaced fluids are completely miscible. This means that interfacial forces can be neglected.

2. The penetrating front is well defined and stable. This requires that diffusion and convective mixing at the interface between the phases is negligible. Diffusion effects will be negligible if $4B^2\bar{v}/(D_{12}L) >> 1$, where B is one-half the gap width between the plates, L is the length of the flow field, v is the average axial velocity, and D_{12} is the diffusivity of fluid "1" in fluid "2."

3. The volumetric flow rate Q is constant at each cross section of the flow; i.e., we have constant rate displacement.

4. The process occurs under quasi-steady conditions; i.e., the problem can be analyzed as a steady state problem at any time. The solution depends on time through the evolution of these steady state solutions.

5. There is only one important component of velocity, namely v_z (or $\hat{v}_z$).

6. The velocity gradients in the z direction are negligible in comparison to the velocity gradients in the radial direction, i.e., the velocity and pressure fields are only dependent on y.

Physically, the last three assumptions imply that at each small region, Δz, (see Figure 2) the flow can be approximated as that of a layer of one fluid moving through another fluid, both in parallel flow.

Subject to these assumptions and interpretations, the equations of motion for the flow in the respective phases reduce to the forms associated with parallel shear flows.[14]

$$\frac{d\hat{\tau}_{yz}}{dy} = -\left[\frac{dp}{dz} + \hat{\rho}g\right], \; y \leqslant \delta \tag{1}$$

$$\frac{d\tau_{yz}}{dy} = -\left[\frac{dp}{dz} + \rho g\right], \; \delta \leqslant y \leqslant B \tag{2}$$

The first equation refers to the displacing fluid and the second to the displaced fluid. The geometrical quantities B and δ are as defined in Figure 1. Each of these equations stems from a force balance between the viscous forces resiting shear, the pressure forces, and the gravitational forces.

In order to relate the viscous shear stresses $\hat{\tau}_{yz}$ and τ_{yz} to the velocity field, a rheological equation of state is required. For drilling muds and cement slurries, an accurate description can be obtained using the rheological model of Robertson and Stiff.[15,16]

$$\hat{\tau}_{yz} = \hat{m}\left[-\frac{d\hat{v}_z}{dy} + \hat{\alpha}\right]^{\hat{n}} \tag{3}$$

$$\tau_{yz} = m\left[-\frac{dv_z}{dy} + \alpha\right]^{n} \tag{4}$$

It should be noted that this model includes the Newtonian fluid model, the Bingham plastic model, and the power-law model as special cases. The yield stresses associated with this description are given by the following.

$$\hat{\tau}_y \equiv \hat{m}\hat{\alpha}^{\hat{n}}, \; \tau_y = m\alpha^n \tag{5}$$

To complete the problem, we must specify the boundary conditions. Here we assume zero stress in the center of the flow channel, continuity of stress and velocity at the interface, and no slip conditions at the wall. These can be summarized as follows.

$$\hat{\tau}_{yz} = 0 \text{ at } y = 0 \tag{6}$$

$$\hat{\tau}_{yz} = \tau_{yz} \text{ at } y = \delta \tag{7}$$

$$\hat{v}_z = v_z \text{ at } y = \delta \tag{8}$$

$$v_z = 0 \text{ at } y = B \tag{9}$$

The specification of the problem is complete, and the solution now proceeds in a fairly direct way.

THE SOLUTION

The solution procedure follows closely that given previously[2], and the detailed steps are given elsewhere.[17] Integration of Equations 1 and 2 with the boundary conditions, Equations 6 and 7, gives the stress fields at any position z in the flow field:

$$\hat{\tau}_{yz} = -\frac{dp}{dz} + \hat{\rho}g \; y, \; y \leqslant \delta \tag{10}$$

$$\tau_{yz} = -\frac{dp}{dz} + \hat{\rho}g \; y - (\hat{\rho}-\rho)\, g\delta, \; \delta \leqslant y \leqslant B \tag{11}$$

or, alternately, in functional form:

$$\hat{\tau}_{yz} = \hat{\tau}_{yz}\, \frac{dp}{dz}, y \; , \; \tau_{yz} = \tau_{yz}\left[\frac{dp}{dz}, y, \delta\right] \tag{12, 13}$$

The substitution of these equations into the rheological descriptions, Equations 3 and 4, coupled with the use of the boundary conditions, Equations 8 and 9, give the velocity fields in both phases, i.e.:

$$\hat{v}_z = \hat{v}_z \; \frac{dp}{dz}, y, \delta \; , \; v_z = v_z\left[\frac{dp}{dz}, y, \delta\right] \tag{14, 15}$$

where we have not bothered to give the lengthy expressions, but just the functional dependence. The dimensionless forms of the actual expressions are summarized in the appendix.

In light of the fact that the volumetric flow rate Q at each cross section of the flow is constant we can obtain:

$$Q = 2\int_0^{\delta} \hat{v}_z W dy + 2\int_{\delta}^{B} v_w W dy$$

or using Equations 14 and 15

$$Q = Q \; \frac{dp}{dz}, \delta \tag{16}$$

Solving for dp/dz and substituting into Equations 14 give:

$$\hat{v}z = \hat{v}z\,(Q, y, \delta) \tag{17}$$

By integrating the velocity of the fluid particles at the interface ($y=\delta$), we can determine the z position of the interface at any time t, assuming z=0 at t=0. The result is:

$$z\,|_{y=\delta} = \int_0^t v_z\,|_{y=\delta}\,dt = z\,(Q,\delta t) \qquad (18)$$

which defines the position of the interface δ as a function of z, Q, and t. This result can be integrated to give the volume displaced as a function of time:

$$V = 2W\int_{\delta=0}^{B} z\,|_{y=\delta}\,d\delta \quad z \leqslant L \qquad (19)$$

where W is the width of the flow system.

Although the solution procedure outlined here is straightforward, the actual expressions and details are quite involved (see the appendix for summary of important equations). At various steps, numerical procedures are required to realize the solution. In particular, the implicit nature of the equation corresponding to Equation 16 above requires a root finding procedure to determine dp/dz for known values of Q and δ. Also, due to the complex form of $z\,|_{z=\delta}$, analytical integration of Equation 19 is not possible, and hence, a numerical integration scheme is needed. Computer programs and detailed descriptions of these calculations have been prepared by Beirute.[17]

Several things about the solution should be noted. First, it is approximate, and hence, the displaced volume calculated to Equation 19 does not necessarily correspond to the actual volume entering at the bottom as calculated by $Q\Delta t$ where Δt corresponds to the elapsed displacement time. (This comparison is only valid up to the time of interfacial penetration at the top of the system). As a result, it is possible that a material balance inconsistency can arise, since the calculated amount of fluid displaced from the system may not correspond to that which actually entered. To correct this problem, we use the same approach used previously[2] and introduce a correction factor ϵ into Equation 19 to account for this effect as follows,

$$V = 2W\epsilon\int_0^{B} z\,|_{y=\delta}\,d\delta \qquad (20)$$

where ϵ is determined by setting $V = Q\Delta t$. Clearly, prior to interfacial penetration at the top of the system, the displacement is simply $Q\Delta t$. However, the time of penetration must be calculated from Equation 18 and subsequent displacement efficiencies (V/2BWL) from Equation 20 with the restriction that the integration is only over the displacing fluid actually in the flow field geometry, i.e., $z \leqslant L$.

To a further point, it should be noted from Figure 2 that $d\hat{v}_z/dy$ and dv_z/dy should both be less than or equal to zero. It then follows from Equations 3, 4, 10 and 11 that

$$\hat{\tau}_{yz} = -\left[\frac{dp}{dz} + \hat{\rho}g\right] y \geqslant 0 \qquad (21)$$

and

$$\tau_{yz} = -\left[\frac{dp}{dz} + \rho g\right] y - (\hat{\rho}-\rho)\,g\delta \geqslant 0 \qquad (22)$$

Here again, because of the approximate nature of the solution, situations can arise where the calculated values of $\hat{\tau}_{yz}$ and τ_{yz} may in fact be slightly negative. Under such conditions, we arbitrarily set $\hat{\tau}_{yz}$ and/or τ_{yz} equal to zero and assume the displacement front to be flat over the regions where this occurs. The physical validity of such an approach is discussed elsewhere.[2,17]

PREDICTIONS OF DISPLACEMENT MODEL

We now wish to consider the displacement results obtained from the displacement model just described. In doing this, we present the results in dimensionless form with the important variables being:

$k_1 \equiv -(dp/dz)/\rho g$ = the dimensionless pressure drop (23)

$k_2 \equiv \hat{\rho}/\rho$ = the density ratio, displacing phase to displaced phase (24)

$k_3 \equiv (\hat{m}/\rho gB)^{1/\hat{n}}/(m/\rho gB)^{1/n}$ = an effective viscosity ratio, displacing phase to displaced phase (25)

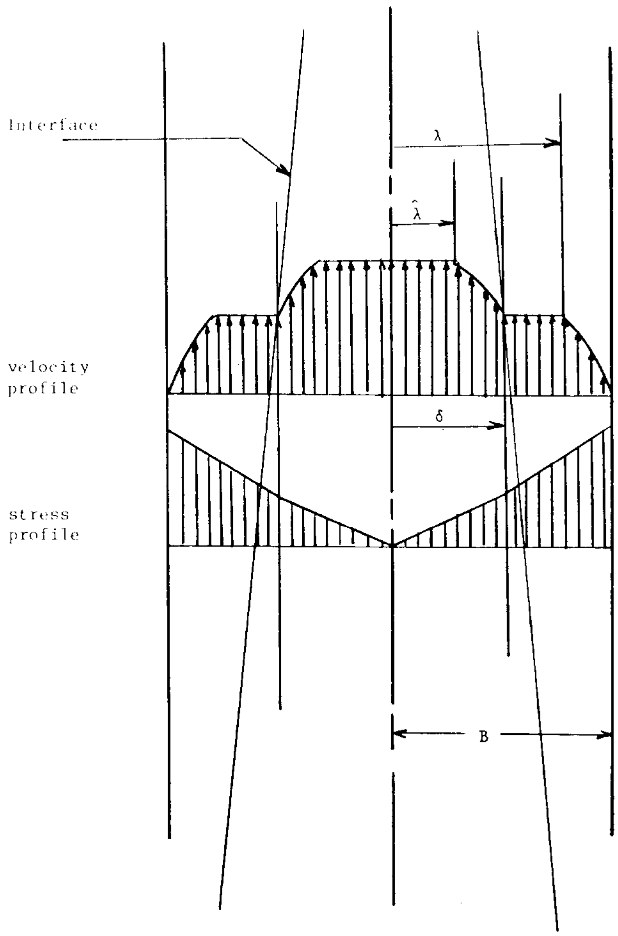

FIGURE 2 VELOCITY AND STRESS PROFILES

$k_4 \equiv Q/\left(2B^2W(\rho gB/m)^{1/n}\right)$ = the dimensionless flow rate (26)

$k_5 \equiv (\tau_y/\rho gB)^{1/n}$ = a dimensionless measure of yield stress of the displaced phase (27)

$k_6 \equiv (\hat{\tau}_y/\rho gB)^{1/n}/k_3$ = a dimensionless measure of yield stress of the displacing phase (28)

$t^* \equiv (Q/2BWL)\,t$ = dimensionless displacement time (29)

$\zeta = z|_{y=\delta}/L$ = dimensionless z position of interface (30)

$V^* = V/2WLB$ = displacement efficiency (31)

It should be noted here that t^* also represents the number of displacement volumes of the displacing fluid injected. Also, the displacement efficiency V^* is equal to t^* up until the penetration time t^*_{pen}. Further, complete displacement corresponds to $V^* = 1.0$, and if $V^* = t^*_{pen} = 1$, the displacement process is optimal. Physically, the later corresponds to plug flow displacement.

Before presenting the results in terms of these variables, there are certain features of the flow field and displacement mechanics which should be discussed. These relate to the various types of displacement flow phenomena which can arise with materials possessing yield stresses.

In particular, from Equations 10 and 11, the stress field across the gap can be sketched as that given in Figure 3(a). In both phases, the stress varies linearly with y with slopes of $-(dp/dz + \hat{\rho}g)$ and $-(dp/dz + \rho g)$ for the displacing and displaced phases, respectively. (Note: $\hat{\rho} \geqslant \rho$ for stable displacements). Now, a number of different flow cases can be visualized depending on whether the yield stresses τ_y and $\hat{\tau}_y$ of the materials are greater or less than $\hat{\tau}_{yz}(\delta)$ and $\tau_{yz}(B)$. For example, if $\hat{\tau}_y \leqslant \tau_{yz}(\delta)$, then the internal phase flow field will be plug flow for all values of $y \leqslant \hat{\lambda}$, where $\hat{\lambda}$ is defined by $\hat{\tau}_{yz}(y) \leqslant \hat{\tau}_{yz}(\hat{\lambda}) = \tau_y$, and a shear flow for values $y > \hat{\lambda}$. A similar situation occurs in the outer phase when $\tau_{yz}(\delta) \leqslant \tau_y \leqslant \tau_{yz}(B)$. In this latter case, the plug and shear flow regions are separated at $y = \lambda$ where the latter is obtained from $\tau_y = \tau_{yz}(\lambda)$. Case 2 represented in Figure 3(b) illustrates the nature of the flow field and displacement process under these conditions. Four other cases can be visualized, and these are also illustrated in the figure. It should be noted that the most efficient displacements will be achieved in cases approximating plug flow displacement (case 5). Poor displacements can be expected in those cases where the inner phase channels through the center of the outer phase (case 3).

Effect of the Density Ratio (k_2)

Figure shows the effect of k_2 on the displacement efficiency as displacement time is increased. As could be expected, the displacement efficiency increases with time, since more displacing fluid is used to remove the external phase. At $t^*=1$, a volume of cement slurry equal to the volume of the annulus has been used. The figure indicates that by increasing the density of the displacing fluid even slightly, the displacement efficiency can be drastically improved even for relatively short displacement times. It is of interest to note that the penetration time increases with k_2. In Figure 4, the penetration time is that value of t^* at which the given curve intercepts the $dV^*/dt^*=1$ line. It should also be noted that the usage of cement slurry excesses can be of some help under certain conditions. However, when the time of penetration is large, cement excess is of little help.

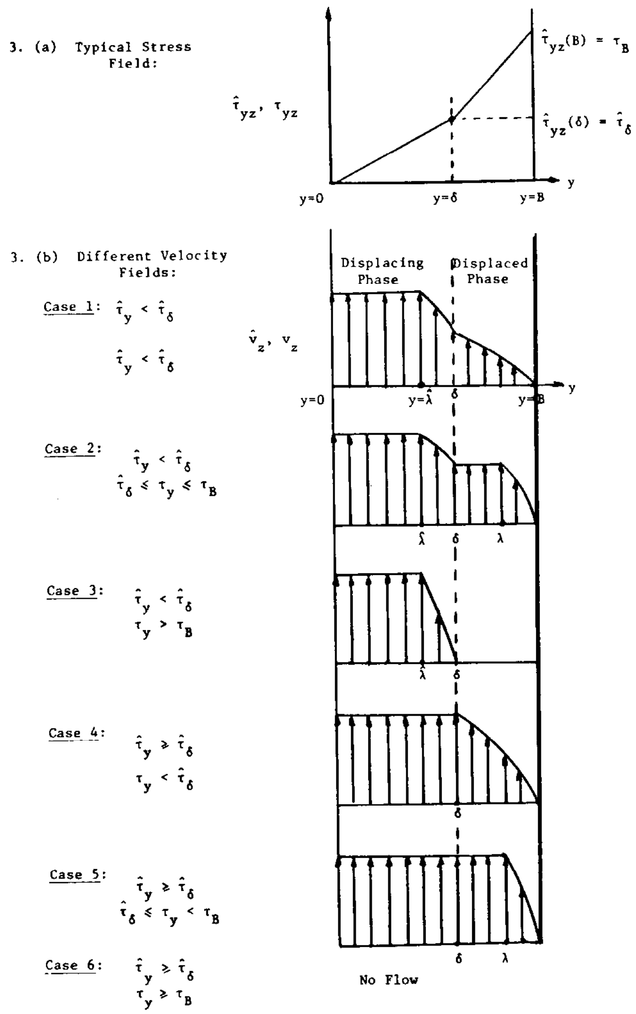

FIGURE 3—POSSIBLE FLOW AND DISPLACEMENT CHARACTERISTICS

Effect of the "Viscosity Ratio" (k_3)

Figure 5 indicates that high values of k_3 are desirable for good displacement efficiencies; all other variables remaining the same. Large k_3 values mean that the displacing phase is more viscous than the displaced phase. The model shows that, for small values of k_3, the penetrating front tends to channel through the center of the flow field, leaving behind a great deal of external phase that could never be removed regardless of the amount of displacing phase used.

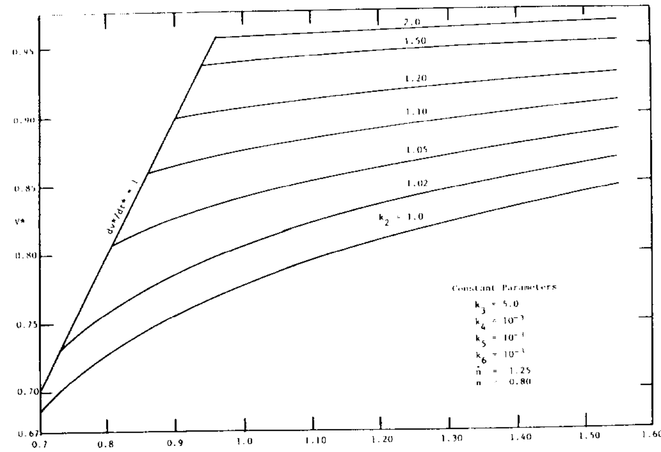

FIGURE 4—EFFECT OF k_2 AND t* ON THE DISPLACEMENT EFFICIENCY

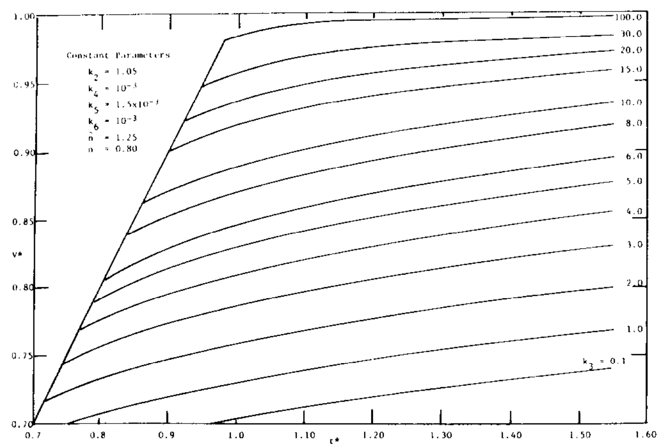

FIGURE 5—EFFECT OF k_3 AND t* ON THE DISPLACEMENT EFFICIENCY

Effect of the Displacement Rate (k_4)

As shown by Flumerfelt[2] for the case of no yield stress in the internal and external phases (k_5, k_6 equal to zero), the effect of k_4 depends on the values of n and $\hat{n}$. However, for values of k_5 and k_6 different from zero, this is no longer the case. Figure 6 shows a decrease in displacement efficiency as k_4 is increased. This effect seems to be independent of the relative values of n and $\hat{n}$. The model clearly shows that a decrease on k_4 readily produces a flat penetrating front which gives extremely good times of penetration and, therefore, very good displacement efficiencies.

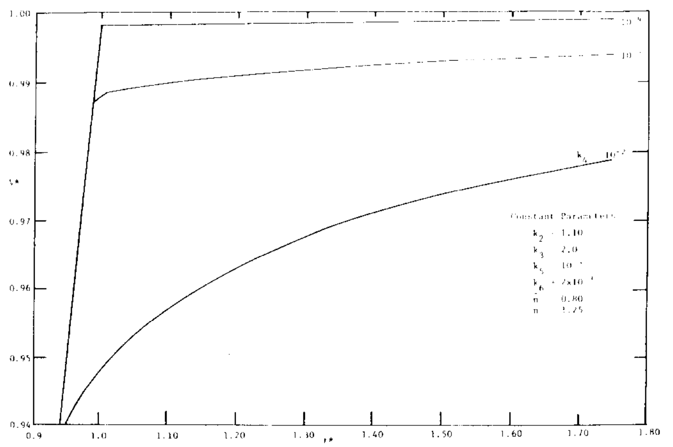

FIGURE 6—EFFECT OF k_4 AND t^* ON THE DISPLACEMENT EFFICIENCY WHEN $\hat{n} < n$ AND THE FLUIDS POSSESS YIELD STRESS.

Effect of the Displaced Phase Yield Stress (k_5)

As k_5 increases, the displacement efficiency decreases. Large values of k_5 mean high yield stresses for the external phase. Penetration times also decrease as k_5 increases. Figure 7 shows that large k_5 values can cause the penetrating front to become very thin, promoting stable channeling, which in turn results in very low displacement efficiencies. The maximum amount of the external phase that can be removed when channeling occurs is (refer to Figure 1):

$$V^*_{max} = \frac{2WL}{2WLB}\delta_f = \frac{\delta_f}{B} \equiv \xi_f \qquad (32)$$

which means that $\left[(1-\xi_f) \times 100\right]$ percent of the external phase (mud) will never be removed.

Effect of the Displacing Phase Yield Stress (k_6)

The displacement efficiency increases as k_6 increases, all the other parameters remaining the same (see Figure 8). Larger values of k_6 mean larger values of the yield stress in the internal phase. Larger yield stresses in the internal phase tend to keep the penetrating front together instead of channeling through the other phase. Figure 9 shows that the penetrating front becomes more blunt as k_6 increases, causing larger penetrating times and, therefore, better displacements. Also, notice that small values of k_6 strongly benefit stable channeling with the consequent low displacement efficiencies.

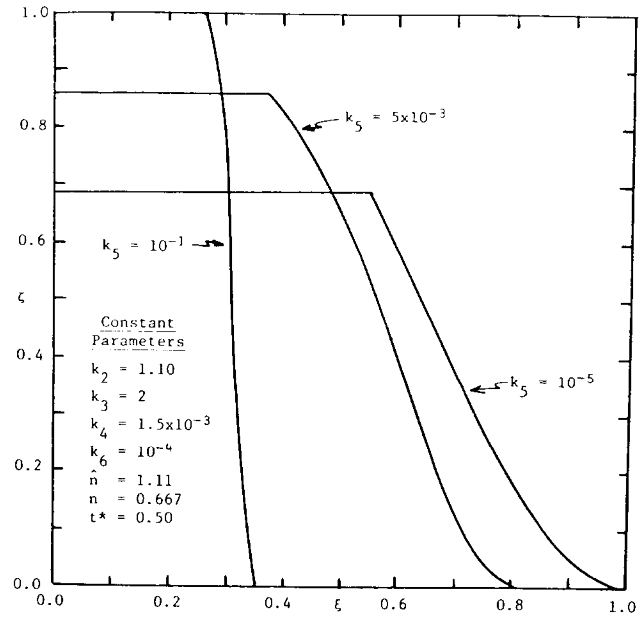

FIGURE 7—EFFECT OF k_5 ON THE SHAPE OF THE PENETRATING FRONT.

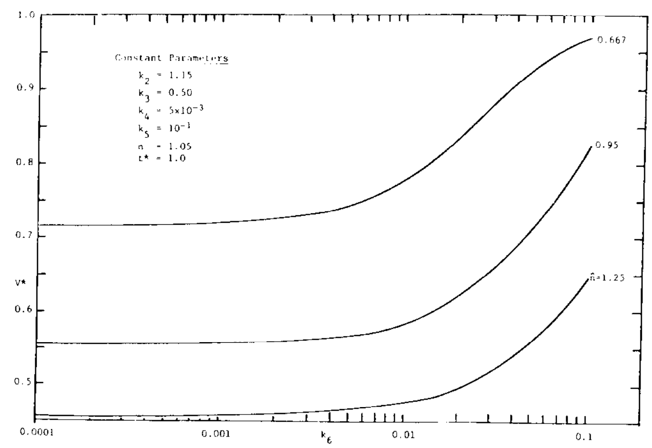

FIGURE 8—EFFECT OF $\hat{n}$ AND k_6 ON THE DISPLACEMENT EFFICIENCY.

Effect of the Flow Behavior Indexes for the Phases

Figure 8 shows that V* (displacement efficiency) decreases as n increases. Therefore, it is desirable to have a displacing phase with small values of $\hat{n}$. The effect of n is contrary to that of $\hat{n}$, as shows in Figure 10. The figure shows an increased tendency to channeling and short penetration times as n decreases.

FIELD APPLICATIONS OF THE MODEL

Two case histories are outlined below:

1. An operator in Fort Bend County, Texas, wanted a good cement around the bottom

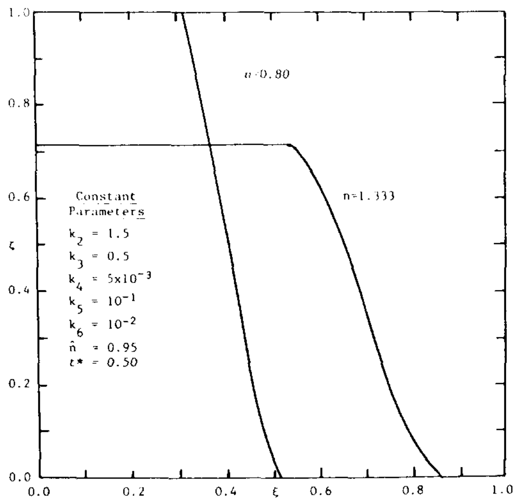

FIGURE 10 EFFECT OF n ON THE SHAPE OF THE PENETRATING FRONT.

1200 feet of a 5 inch casing set in a 9 7/8 inch hole. However, due to well conditions, he could not use a heavy, high-strength cement. Since the mud weight was only 10 lb/gal, the job was performed using 130 barrels of a 13 lb/gal cement slurry. The cement was pumped at 6 BPM. Tests run on the job (radioactive tracer survey) indicated possible cement channeling.

This cementing operation was simulated in the computer using our program. The model predicted a fairly flat penetrating front with a relatively high percent of mud removal. However, it also predicted that the cement would not be able to completely sweep the casing and formation, leaving behind a film of mud on the walls of the annulus.

2. A South Texas well needed to be cemented at 14000 feet. The hole size was 8 1/2 inches, and the casing size was 5 1/2 inches. The mud weight was 18 lb/gal. The well was cemented using a total of 320 barrels of a water external cement slurry. Fifty barrels of a water external emulsion spacer were pumped ahead of the slurry.

   This time the model showed a less blunt penetrating front than for case history 1 but with the cement slurry moving completely against the casing and formation walls. The displacement efficiency was predicted at 91 percent. The results from the field (CBL) indicated very good cement bond through the entire cemented interval.

CONCLUSIONS

1. The development of this model has provided a basis for specifying the relationship between displacement efficiency and the relative densities of the mud and cement, their full rheological behavior, the geometry of the well, and the displacement rate. The model allows the user to investigate the effects of property changes, rate changes, and the like, in order to design a cement job prior to actual field application. The results obtained agree with previous work with regard to the effect of density ratio and viscosities on the displacement efficiency.
2. The study shows that the yield stresses are quite critical in the displacement process. The model predicts that serious cement channeling through the mud will occur if the yield stress of the mud is significantly greater than that of the cement.
3. Field cases agree quite well with the results predicted using the model.
4. The model shows that when the displacement process is properly designed, large amounts of cement slurry (excess) are not needed to achieve good displacement efficiencies. Under certain conditions (generally for displacement cases with low efficiency) the use of cement excess can be of some advantage. However, in the latter cases, turbulent displacement would probably be the best alternative.

NOMENCLATURE

B	=	one-half the gap between the parallel plates
g	=	acceleration of gravity
L	=	length of the parallel plates
m, m	=	"consistency index" in the Robertson-Stiff model, external and internal phase respectively.

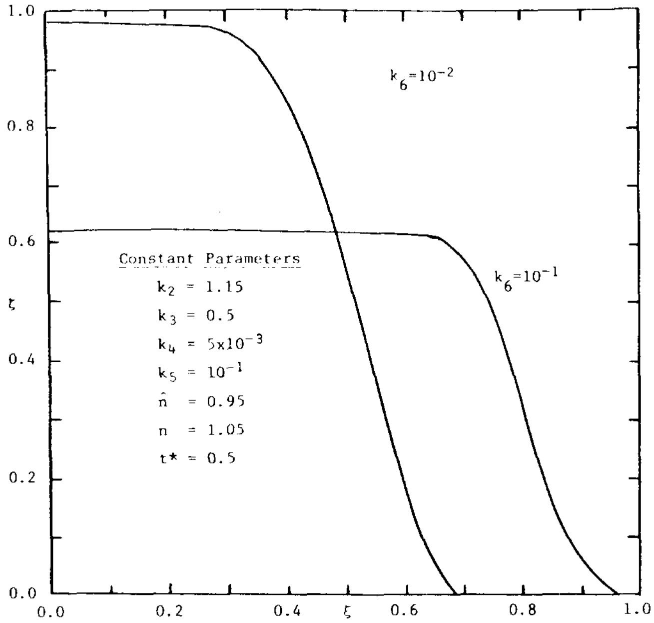

FIGURE 9 EFFECT OF k_6 ON THE SHAPE OF THE PENETRATING FRONT.

n, $\hat{n}$ = "flow behavior index", external and internal phase. Robertson-Stiff model.

P = pressure

Q = volumetric flow rate

t = time

t_{pen} = time of penetration

v_z, $\hat{v}_z$ = velocity components, z direction, displaced (external) and displacing (internal) phase respectively

V = displacement volume

V_a = true volume displaced

W = width of the parallel plates (x direction)

x,y,z = rectangular cartesian coordinates

z = axial position of the interface

α, $\hat{\alpha}$ = shear rate correction constants in the Robertson-Stiff rheological model (external and internal phase respectively)

γ = shear rate

δ = radial position of the interface

ϵ = correction factor to the mass balance inconsistency

ξ_f = maximum thickness of the penetrating front

ξ_L = value of ξ at which the penetrating front intercepts the upper boundary of the flow field

ξ_m = thickness of the tip of the penetrating front

λ, $\hat{\lambda}$ = thickness of the plug flow region, external and internal phase respectively

ρ, $\hat{\rho}$ = density, displaced and displacing phase respectively

ϕ = shape function of the displacement front

τ_{yz}, $\hat{\tau}_{yz}$ = shear stress, displaced and displacing phase respectively

τ_y, $\hat{\tau}_y$ = yield stresses, external and internal phase respectively

Other Dimensionless Groups

A = $(k_2-1)/(k_1-1)$

s = $1/n$

$\hat{s}$ = $1/\hat{n}$

v_z^* = $v_z/(\rho g B/^{n+1}/m)^{1/n}$

$\hat{v}_z^*$ = $\hat{v}_z/(\rho g B^{n+1}/m)^{1/n}$

y^* = y/B

λ^* = λ/B

$\hat{\lambda}^*$ = $\hat{\lambda}/B$

ξ = δ/B

τ_{yz}^* = $\tau_{yz}/\rho g B$

$\hat{\tau}_{yz}$ = $\hat{\tau}_{yz}/\rho g B$

τ_y^* = $\tau_y/\rho g B = m\alpha^n/\rho g B$

$\hat{\tau}_y^*$ = $\hat{\tau}_y/\rho g B = \hat{m}\hat{\alpha}^{\hat{n}}/\rho g B$

APPENDIX

Summary of Important Dimensionless Equations

Next are the most important equations needed for the computer simulation of the model. Detailed development of the equations and additional information is given elsewhere.[17]

Stress Profile

$$\hat{\tau}_{yz}^* = (k_1-k_2)y^*, \quad y^* \leq \xi \tag{1}$$

$$\tau_{yz}^* = (k_1-1)y^* - (k_2-1)\xi,$$

$$\xi \le y^* \le 1 \quad (2)$$

$$\hat{\tau}^*_{yz} \ge 0, \quad \tau^*_{yz} \ge 0 \quad (3)$$

Equation 3 is a calculational restriction on equations 1 and 2.

Thickness of the Plug Flow Regions

$$\hat{\lambda}^* = \begin{matrix}\text{smaller}\\ \text{value of}\end{matrix} \quad \hat{\tau}^*_o/(k_1-k_2) \quad \text{or} \quad \xi \quad (4)$$

$$\lambda^* = \begin{matrix}\text{smaller}\\ \text{value of}\end{matrix} \quad \left(\tau^*_o + (k_2-1)\xi\right)/(k_1-1) \text{ or } 1 . \quad (5)$$

Velocity Profile

$$v^*_z = -\frac{(k_1-1)^s}{(s+1)} \left\{ (y^*-A\xi)^{s+1} - (1-A\xi)^{s+1} \right\}$$

$$-k_5(1-y^*), \quad \lambda^* \le y^* \le 1 \quad \ldots\ldots\ldots \quad (6)$$

$$\hat{v}^*_z = \frac{-(k_1-1)^s}{(s+1)} \left\{ (\lambda^*-A\xi)^{s+1} - (1-A\xi)^{s+1} \right\}$$

$$\frac{-(k_1-k_2)^{\hat{s}}}{(\hat{s}+1)k_3} (y^{*\hat{s}+1} - \xi^{\hat{s}+1}) - k_5(1-\lambda^*) - k_6(\xi - y^*),$$

$$\xi^* < y^* \le \hat{\lambda}^* \quad \ldots\ldots\ldots \quad (7)$$

In the regions $\lambda^* < y^* \leqslant \xi$ and $\hat{\lambda}^* < y^* \leqslant 0$ the velocity is constant and can be obtained from equations 6 and 7 by setting $y^* = \lambda^*$ and $y^* = \hat{\lambda}^*$ respectively.

Volumetric Flow Rate

$$k_4 = \frac{(k_1-k_2)^{\hat{s}}}{(\hat{s}+2)k_3} (\xi^{\hat{s}+2} - \hat{\lambda}^{*\hat{s}+2})$$

$$-\frac{(k_1-1)^s}{(s+1)} \left\{ (\lambda^*-A\xi)^{s+1}\lambda^* - (1-A\xi)^{s+1} \right.$$

$$\left. + \frac{1}{s+2}\left[(1-A\xi)^{s+2} - (\lambda^*-A\xi)^{s+2}\right] \right\}$$

$$-\frac{k_5(1-\lambda^{*2})}{2} - \frac{k_6(\xi^2-\hat{\lambda}^{*2})}{2} \quad (8)$$

This equation is the equivalent to equation 16 in the text of this paper.

Maximum Thickness of the Penetrating Front

$$\xi_f = \frac{(k_1-1)-\tau^*_y}{(k_2-1)} \quad (9)$$

$$k_4 = \frac{(k_1-k_2)^{\hat{s}}}{(\hat{s}+2)k_3} \left\{ \xi_f^{\hat{s}+2} - \hat{\lambda}^{*\hat{s}+2} \right\} - \frac{k_6}{2}(\xi_f^2 - \hat{\lambda}^{*2}) \quad (10)$$

Notice that if $\lambda_f < 1$, stable channeling will occur.

Axil Position of the Penetrating Front

$$\zeta(\xi) = \phi(\xi)t^* \quad \ldots\ldots\ldots \quad (11)$$

$$\phi(\xi) = \frac{1}{k_4} \left\{ \frac{(k_1-1)^s}{(s+1)} \left((1-A\xi)^{s+1} - (\lambda^*-A\xi)^{s+1} \right) - k_5(1-\lambda^*) \right\} \quad (12)$$

$\phi(\xi)$ is known as the shape function of the penetrating front.

Time of Penetration

$$t^*_{pen} = \frac{k_4}{\frac{(k_1-1)^s}{(s+1)} \left((1-A\xi_m)^{s+1} - (\lambda^*-A\xi_m)^{s+1} \right) - k_5(1-\lambda^*)} \quad \ldots \quad (13)$$

See Figure 1 for physical interpretation of ξ_m.

Displacement Efficiency

$$V^* = \xi_m \xi_m + \int_{\xi_m}^{\xi_f} \zeta d\xi, \quad t^* \le t^*_p, \quad \xi_m \ne 0 \quad \ldots \quad (14)$$

$$V^* = \xi_L + \int_{\xi_L}^{\xi_f} \zeta d\xi, \quad t^* > t^*_p \quad (15)$$

REFERENCES

1. Clark, C.R. and Carter, L.G.: "Mud Displacement with Cement Slurries," *J. Pet. Tech.* (July 1973)
2. Flummerfelt, R.W.: "Laminar Displacement of Non-Newtonian Fluids in Parallel Plate and Narrow Gap Annular Geometries," *Soc. Pet. Eng. J.* (April 1975)
3. Graham, H.L.: "Rheology-Balanced Cementing Improves Primary Success," *Oil and Gal J.* (Dec. 1972)
4. McLean, R.H., Manry, C.W. and Whitaker, W.W.: "Displacement Mechanics in Primary Cementing," *J. Pet. Tech.* (1967) 240, 215.
5. Beirute, R.M.: "All Purpose Cement Mud Spacer," Second Symposium on Formation Damage Control, Houston, Texas (1976)
6. Garvin, T., *et al.*: "Scale Model Displacement Studies to Predict Flow Behavior During Cementing," *J. Pet. Tech.* (Sept. 1971)
7. Slagle, K.A.: "An Approach to Designed Cementing Operations Utilizing Rheological Properties of Slurries," 36th SPE of AIME Meeting, Dallas (Oct. 1961)
8. Parker, P.N., *et al.*: "An Evaluation of a Primary Cementing Technique Using Low Displacement Rates," 40th SPE of AIME Meeting, Denver, Colorado (Oct. 1965)
9. Parker, P.N.: "Cementing Successful at Low Displacement Rates," *World Oil* (Jan. 1969)

10. Ross, W.M.: "Low Rate Displacement Solves Tough Cementing Jobs," *Pet. Eng.* (Nov. 1965)
11. Ritter, J.E.: "Viscous Fluid Mud Displacement Technique," SPE Rocky Mountain Meeting, Casper, Wyoming (May 1967)
12. Smith, G.: "Application of Marker and Cell Method to Multiphase Flow Problems," M.S. Thesis Chemical Engineering Department, University of Houston (1975)
13. Cameron, A.: "The Principles of Lubrication," John Wiley and Sons, Inc., New York (1966)
14. Bird, R.B., Stewart, W.E. and Lightfoot, E.N.: "Transport Phenomena," John Wiley & Sons, New York (1966) 7th Edition
15. Robertson, R.E. and Stiff, H.A.: "An Improved Mathematical Model for Relating Shear Stress to Shear Rate in Drilling Fluids and Cement Slurries," *Soc. Pet. Eng. J.* (Feb. 1976)
16. Beirute, R.M. and Flumerfelt, R.W.: "An Evaluation of the Robertson-Stiff Model Describing Rheological Properties of Drilling Fluids and Cement Slurries," *Soc. Petr. Eng. J.* (April 1977)
17. Beirute, R.M.: "Miscible Displacement of Viscous, Non-Newtonian Fluids in Different Geometries. An Analytical Approach," Ph.D. Dissertation, Chemical Engineering Department, University of Houston (May 1977)

ACKNOWLEDGMENT

One of the authors, Robert M. Beirute, wishes to acknowledge the Management of The Western Company of North America for the assistance and moral support while carrying on Ph.D. studies at the University of Houston, which led to the thesis from which this paper was extracted.